Lyotropic Liquid Crystallinity of Linear and Star Poly(quinoxaline-2,3-diyl)s: Isotropic-Liquid Crystal Phase Equilibria in Tetrahydrofuran

Hirokazu Hasegawa,[†,‡] Ken Terao,[†] Takahiro Sato,[†] Yuuya Nagata,[§] and Michinori Suginome[§]*

[†]Department of Macromolecular Science, Graduate School of Science, Osaka University, 1-1 Machikaneyama-cho, Toyonaka, Osaka 560-0043, Japan
[‡]Materials Characterization Laboratories, Toray Research Center, Inc., 3-3-7, Sonoyama, Otsu, Shiga 520-8567, Japan
[§]Department of Synthetic Chemistry and Biological Chemistry, Graduate School of Engineering, Kyoto University, Katsura, Kyoto 615-8510, Japan

* Corresponding author. Tel.: +81 6 6850 5459; fax: +81 6 6850 5461.
E-mail address: kterao@chem.sci.osaka-u.ac.jp

ABSTRACT: Lyotropic liquid crystallinity was investigated for concentrated solution of linear and 3-arm star poly(quinoxaline-2,3-diyl) of which main chain has a rigid helical nature in tetrahydrofuran. Four samples both for linear and star chains were prepared with the weight-average molar mass M_w ranging from 50 to 250 kg mol^{-1}. Two phase boundary concentrations, c_I between the isotropic and biphasic regions and c_A between the biphasic and anisotropic regions, were determined as a function of M_w. The resultant c_I and c_A for the linear chain increased gradually with lowering M_w. This behavior was successfully explained by the latest theory for lyotropic liquid crystallinity based on the scaled particle theory (SPT) for the wormlike spherocylinder. The phase diagram for star chains, on the other hand, has similar c_I and c_A at high M_w region but increased abruptly with decreasing M_w. It can be explained by a modified SPT theory in which we assumed two or three arm chains align parallel in the nematic phase. Small-angle X-ray scattering pattern for the concentrated solutions indicated that smectic superstructure was contained at least a little in the liquid crystalline phase and the diffraction peak of the linear chains corresponded to the total chain length while the *d*-spacing for the star chain is almost the same as that for the arm length, supporting the above mentioned assumption for the modified SPT.

Key Words: Stiff chains, star polymer, lyotropic liquid crystallinity, phase diagram, scaled particle theory, small-angle X-ray scattering

Introduction

One of the characteristic feature of stiff chains is lyotropic liquid crystallinity.[1] Indeed, various stiff polymers consisting of π-bond nature, *e.g.*, poly(1,4-benzamide),[2] poly(isocyanate)s,[3-6] and poly(carbodiimide)s[7-8] have been reported to exhibit lyotropic liquid crystallinity in concentrated solutions. Polymer chains spontaneously align in the liquid crystalline phase, and the orientational state is responsive to external electric and flow fields. Such behavior can be applied to produce strong fibers, electro-optical devices, actuators, and so on.[9] Concentrated solution of such stiff chains forms liquid crystal phase above the phase boundary concentration. This phase boundary concentration depends on the chain length, stiffness, and thickness including

the intermolecular interactions between the polymer chains, but is insensitive generally to the temperature comparing with flexible polymer – poor solvent systems. The phase boundary concentration has therefore been widely investigated for many linear polymers as a function of the molar mass of the polymer.[10-16]

Poly(quinoxaline-2,3-diyl)s are classified to as a helical polymer[17] of which internal rotation of the main chain is significantly restricted in solution and thus applied for various asymmetric reactions.[18-20] Indeed, a poly(quinoxaline-2,3-diyl), that is, poly[5,8-dimethyl-6,7-bis(propoxymethyl)quinoxaline-2,3-diyl] (LPQ) behaves as a stiff chain of which the Kuhn segment length λ^{-1} (or twice the persistence length) was estimated to be 43 nm in tetrahydrofuran (THF), which is a good solvent of LPQ.[21] This value is similar to that for poly(*n*-hexyl isocyanate) of which λ^{-1} was reported to be 42 – 84 nm appreciably depending on the solvents.[22-24] Indeed, another poly(quinoxaline-2,3-diyl) with chiral side groups shows cholesteric superstructure in the cast film,[25] and certain achiral poly(quinoxaline-2,3-diyl)s exhibit thermotropic liquid crystalline phase.[26] Moreover, we found LPQ samples have liquid crystalline phases in THF in our preliminary experiments. Concentrated solutions of LPQ in THF are good models to investigate thermodynamics of lyotropic liquid crystallinity of stiff polymer chains.

The liquid crystal state should also depend on the polymer chain architecture. For example, Zakharova et al.[27] reported that phase boundary concentration of supercoiled cyclic DNA is appreciably different from those for linear DNA, and furthermore, we recently found that a rigid ring polysaccharide derivative has somewhat higher phase boundary concentration than that for the corresponding linear polymer.[28] Similar high boundary concentration was also found for star-branched poly(*n*-hexyl isocyanate).[29] Quantitative phase diagram for nonlionear rigid polymers is however limited.

Recently, we successfully synthesized 3-arm star poly[5,8-dimethyl-6,7-bis(propoxymethyl)quinoxaline-2,3-diyl] (A3PQ) by means of the core first method with a tri-functional initiator.[30] Since this polymer behaves as rigid star chain in THF, a good solvent, it is a good model for star branched polymer chains consisting of rigid part chains. We thus investigated molar mass dependence of the isotropic-liquid crystal phase boundary concentrations for THF solutions of LPQ and A3PQ of which chemical structures are shown in Chart 1. The obtained data were analyzed in terms of the scaled particle theory (SPT) for the wormlike spherocylinder[10] to elucidate thermodynamic features of concentrated solutions of linear and star-shaped stiff polymer chains. Small-angle X-ray scattering measurements for concentrated THF solutions both for LPQ and A3PQ were also made to obtain the structural information of the liquid crystalline phase.

Chart 1. Chemical Structures of LPQ and A3PQ.

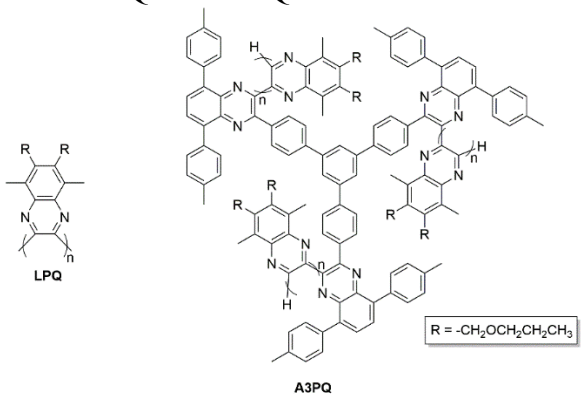

Experimental Section

Samples. Previously investigated four A3PQ samples, **A3PQ-40**, **A3PQ-80**, **A3PQ-160**, and **A3PQ-240**, were used in this study. Their weight-average molar mass M_w ranges from 53 to 245 kg mol^{-1}, which corresponds to the degree of polymerization for each side chain to be between 60 and 270. The dispersity index $Đ$ defined as the ratio of M_w to the number-average molar mass were less than 1.2. We further synthesized four LPQ samples, **LPQ-200**, **LPQ-400**, **LPQ-600**, and **LPQ-800**, for which M_w and $Đ$ values were estimated in terms of the size-exclusion chromatography equipped with a multi-angle light scattering detector and a viscosity detector as reported elsewhere.[21] The resultant M_w values are summarized in Table 1 along with those for A3PQ samples. The $Đ$ values were 1.03, 1.04, 1.04, and 1.08 for **LPQ-200**, **LPQ-400**, **LPQ-600**, and **LPQ-800**, respectively. Similar values were obtained from the universal calibration method.[31-33]

Table 1. Weight-average Molar Mass M_w and the Phase Boundary Concentrations (c_I and c_A) of the LPQ and A3PQ Samples in THF at 25 °C

Sample	M_w (kg mol^{-1})	c_I (g cm^{-3})	c_A (g cm^{-3})
LPQ-200	59.1 [a]	0.296	0.332
LPQ-400	118 [a]	0.267	0.321
LPQ-600	182 [a]	0.262	0.309
LPQ-800	243 [a]	0.254	0.306
A3PQ-40	52.9 [b]	0.506	0.574
A3PQ-80	88.8 [b]	0.384	0.452
A3PQ-160	176 [b]	0.292	0.382
A3PQ-240	245 [b]	0.272	0.330

[a] From SEC-MALS. [b] Ref. 30.

Phase Boundary Concentration Measurements. Two phase boundary concentrations, c_I between the isotropic and biphasic regions and c_A between the biphasic and anisotropic regions, were determined both for LPQ and A3PQ samples with the following procedure. Their concentrated solutions were prepared in a sealed glass tube of which volume was calibrated with water as a function of the meniscus height. The initial concentration c_0 was chosen to be between 0.257 and 0.311 g cm^{-3} for LPQ and between 0.271 and 0.572 g cm^{-3} for A3PQ. The value of c_0 was determined from the weight fraction of polymer sample in solution with the solution density ρ. The ρ value was calculated with the partial specific volume $\bar{v}$ which was determined to be 0.896 cm^{3}g^{-1} for **A3PQ-80** from the solution density measurements by using a DMA-60 densitometer (Anton-Paar, Austria). The solution was heated to 40 °C to dissolve the polymer sample completely and centrifuged at 4,000 rpm for 2 – 6 h at room temperature (approximately equal to 25 °C) to achieve a complete phase separation. The glass tube was placed in a thermostated water bath at 25 °C to determine both position of the meniscus and the boundary

between isotropic and anisotropic phases by using a traveling microscope with a digital micrometer to determine the volume fraction Φ_{LC} of the anisotropic phase in the total solution.

Small-angle X-ray Scattering (SAXS). SAXS measurements were made for concentrated LPQ and A3PQ solutions in THF at the BL40B2 beamline in SPring-8 (Hyogo, Japan) or at the BL-6A beamline in KEK-PF. The combination of the wavelength and the camera length were chosen to be 0.077 nm and 0.50 m (BL40B2), 0.10 nm and 4 m (BL40B2), and 0.15 nm and 2.5 m (BL-6A). An R-AXIS VII imaging plate detector (BL40B2) or a Dectris PILATUS3 1M silicon pixel detector (BL-6A) were used to obtain the scattering intensity I as a function of the magnitude q of the scattering vector with our homemade software or SAngler.[34] The actual camera length was determined from the diffraction peak of silver behenate. Sample solutions were prepared in glass capillaries with the diameter of 2 mm. The capillary was centrifuged to obtain uniform solution.

Results and Discussion

Phase Diagram. Figure 1 displays photographs of a biphasic THF solution of an A3PQ sample after centrifugation, without polarizers and under crossed-Nicols condition. It can be seen that almost complete phase separation is achieved with an anisotropic bottom phase, indicating that the volume fraction Φ_{LC} is accurately determined. As shown in Figure 2, plots of c_0 against Φ_{LC} for all LPQ and A3PQ samples are almost linear. The phase boundary concentrations c_I and c_A were therefore determined as the extrapolation values of c_0 to $\Phi_{LC} = 0$ and $\Phi_{LC} = 1$, respectively.

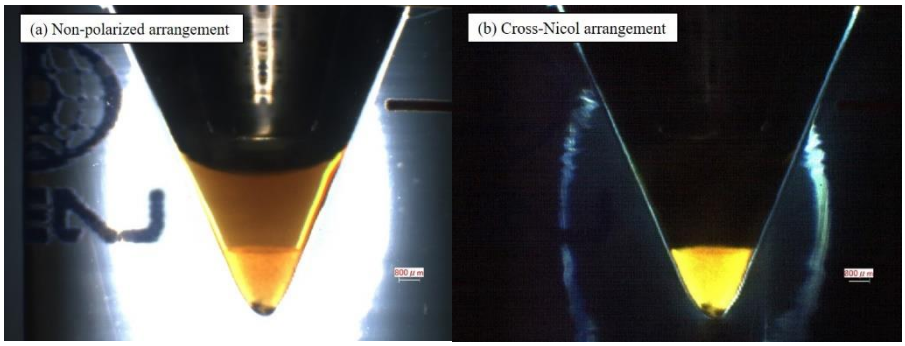

Figure 1. Photographs for coexistence phases of **A3PQ-80** in THF at 25 °C (c_0 = 0.398 g cm^{-3}). (a) Non-polarized image. (b) Crossed-Nicols image.

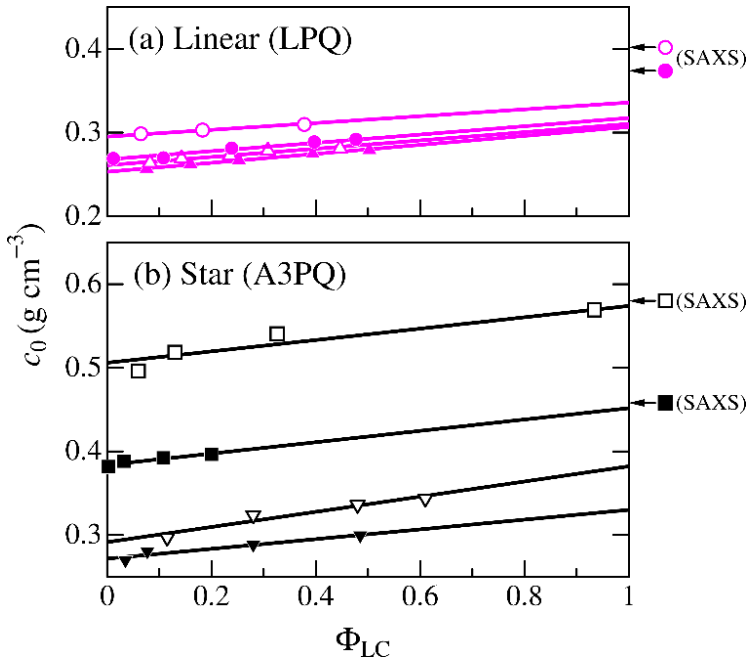

Figure 2. Plots of c_0 vs Φ_{LC} for LPQ (a) and A3PQ (b) samples in THF at 25°C for **LPQ-200** (unfilled circles), **LPQ-400** (filled circles), **LPQ-600** (unfilled triangles), **LPQ-800** (filled triangles), **A3PQ-40** (unfilled squares), **A3PQ-80** (filled squares), **A3PQ-160** (unfilled inverted triangles), and **A3PQ-240** (filled inverted triangles). Arrows indicate the polymer mass concentration for SAXS measurements (see Figure 6).

Numerical c_I and c_A data for LPQ and A3PQ samples are summarized in the third and fourth columns in Table 1 and the M_w dependence is illustrated in Figure 3. Both c_I and c_A for LPQ slightly increase with lowering M_w in the investigated M_w range. This is a typical behavior for the semiflexible chains for relatively high M_w samples.[10] On the other hand, those for the star polymer, A3PQ, are significantly higher than those for the corresponding linear chain at low M_w range. This is consistent with the previous result for 3-arm star poly(*n*-hexyl isocyanate), which has qualitatively higher phase boundary concentrations than those for the linear analogue.[29] Another interesting feature is that the phase boundary concentrations decrease abruptly with increasing M_w and the difference in the phase diagram between linear and star chains becomes mostly insignificant at high M_w even though chain dimensions between star and linear chains appreciably different even for the highest molar mass sample.[30] This is a similar behavior at least experimentally to those for flexible chains, that is, both critical solution temperature for four-arm[35] and six-arm[36] star polystyrene in a theta solvent, cyclohexane, approaches to the identical theta temperature of linear polystyrene with increasing M_w.

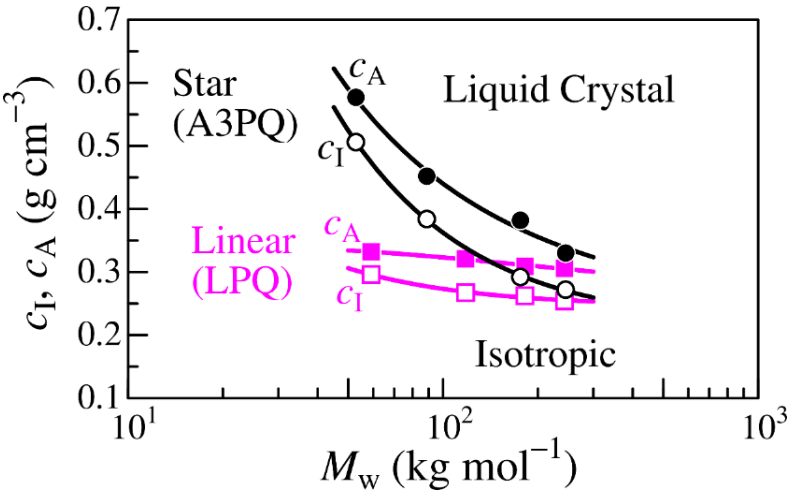

Figure 3. M_w dependence of c_I (unfilled symbols) and c_A (filled symbols) for LPQ (squares) and A3PQ (circles) in THF at 25 °C.

X-ray Diffraction. As mentioned above, SAXS measurements were made for all LPQ samples, **A3PQ-40**, and **A3PQ-80** in THF at 25 °C. Concentration of the solution was set to be higher than c_A, between 0.32 and 0.58 g cm^{-3}. A broad peak is found for each sample between 2.5 – 3.5 nm^{-1}, corresponding to 1.8 – 2.5 nm of the lattice spacing. A small sharp peak for A3PQ might be due to the inhomogeneity of the solution since c of the A3PQ samples was somewhat higher than those for LPQ. If we consider this diffraction is owing to the spacing of the hexagonal packing, the peak position should be proportional to $c^{1/2}$. Plots of I vs $q\,c^{-1/2}$ are thus shown in Figure 4(b). Interestingly, the peak position is substantially close to $q\,c^{-1/2} = 5.0 \times 10^7$ g$^{-1/2}$cm$^{1/2}$ both for linear and star polymers, suggesting at least locally that chain alignment in the liquid crystalline phase are insensitive to the polymer architecture and the chain length. In other words, star polymer chains may align linearly as illustrated in Figure 5(a) and 5(b) while another conformation in Figure 5(c) should also be found in the isotropic phase. This is possible for the current star polymer because particle scattering function of A3PQ in dilute solution were well explained by the wormlike star chain with a universal joint at the branching point[30].

For complete hexagonal packing for rigid rod polymers, the distance a between adjacent rods can be written as

$$a = \sqrt{\frac{2M_0}{\sqrt{3}N_A hc}} \tag{1}$$

where N_A, M_0, and h are the Avogadro number, the molar mass of the repeat unit (M_0 = 0.300 kg mol^{-1}), and the helix pitch per residue (h = 0.19 nm). If we utilize the Bragg raw, $a = 2\pi / q_c$, with q_c being q at the peak, $q_c\,c^{-1/2}$ for the hexagonal packing rods can be calculated from the following expression

$$q_c c^{-1/2} = \pi\sqrt{\frac{2\sqrt{3}N_A h}{M_0}} \tag{2}$$

From this equation, the calculated value of $q_c\,c^{-1/2} = 3.6 \times 10^7$ g$^{-1/2}$cm$^{1/2}$ is somewhat smaller than that for the experimental data. Taking into consideration that the $q\,c^{-1/2}$ value for the tetragonal packing ($q_c\,c^{-1/2} = 3.9 \times 10^7$ g$^{-1/2}$cm$^{1/2}$) is still smaller, this difference might be due to gaps between two polymer chains between the chain ends.

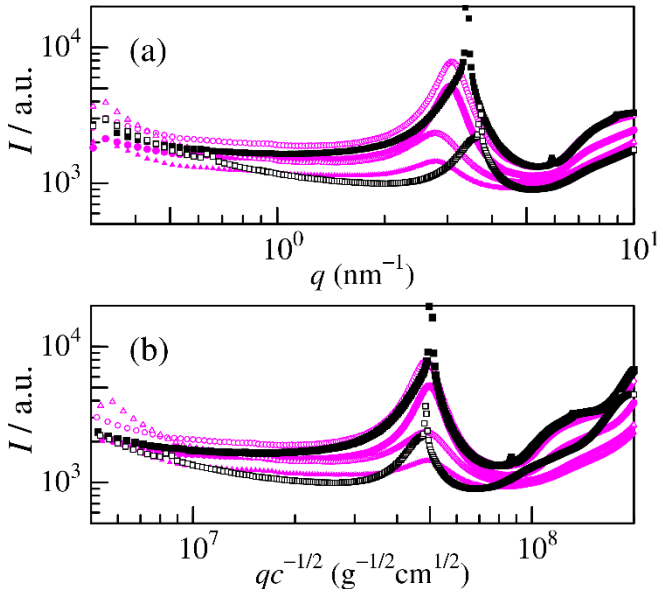

Figure 4. (a) Angular dependence of scattering intensity I for **LPQ-200** (unfilled circles, $c = 0.40_2$ g cm^{-3}), **LPQ-400** (filled circles, $c = 0.37_4$ g cm^{-3}), **LPQ-600** (unfilled triangles, $c = 0.32_5$ g cm^{-3}), **LPQ-800** (filled triangles, $c = 0.31_8$ g cm^{-3}), **A3PQ-40** (unfilled squares, $c = 0.58_0$ g cm^{-3}), and **A3PQ-80** (filled squares, $c = 0.45_8$ g cm^{-3}) all in THF at 25 °C. (b) Plots of I vs $qc^{-1/2}$.

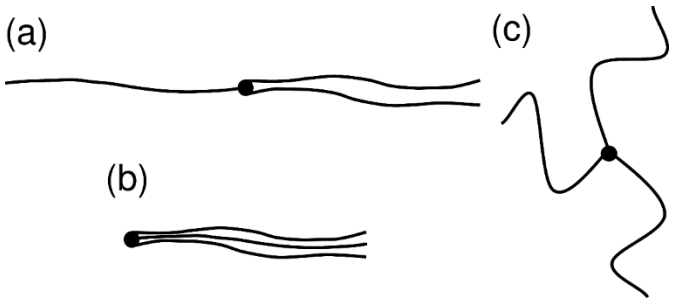

Figure 5. Schematic representation of two suggested conformations of A3PQ chains in liquid crystal phase (a) (b) and a possible conformation in isotropic phase (c). Filled circles indicate the branching point.

Small diffraction peaks at lower q region were found for four samples, **LPQ-200**, **LPQ-400**, **A3PQ-40**, and **A3PQ-80**, as shown in Figure 6. The first peak for the two LPQ samples corresponds to the d-spacing D of 41 and 83 nm for **LPQ-200** and **LPQ-400**, respectively. These values are substantially close but about 10 % longer than those for the corresponding contour length L, that is, 37 nm and 74 nm, estimated from dilute solution properties.[21] These peaks thus suggest the formation of smectic layer. The q values for the second, third, and forth peaks are twice, three times, and four times of the first peak, supporting the smectic structure. Although smectic phases were also found for poly(γ-benzyl α,L-glutamate),[37] poly(dialkylsilane),[38] and amylose derivatives,[16] to the best of our knowledge, this is the first example for the synthetic helical polymer exhibiting smectic phase without using the bacterial or enzymatic polymerization, or the molecular weight fractionation, but sorely using the living polymerization with a transition metal initiator. It is however noticed that the smectic structure of LPQ may not be major around c_I and c_A because the diffraction peak for LPQ at high q range (Figure 4) is broad and c_A is smaller

than those for the diffraction measurements. On the contrary, smectic phase for amylose tris(*n*-butylcarbamate) has a sharp diffraction at high q range.[16]

For star polymer samples, a less significant peak is found for each sample in Figures 6(c) and 6(d), also suggesting the existence of the smectic layer. The *d*-spacing (D) of the peak is calculated to be 9.7 nm and 20 nm for **A3PQ-40** and **A3PQ-80**, respectively. These values are almost the same as those for the contour length L_s of each arm ($L_s \equiv L/3$) of which the values are shown in the figure. It is consistent with the two conformations shown in Figure 5(a) and 5(b) in the liquid crystalline phase. These peaks for A3PQ samples were also found for another measurement which was acquired one month later than the original measurement, thus the structure is stable. The smectic peaks are less significant, when the concentration is close to c_A (cf. arrows on the right-hand side of Figure 2), so that the smectic structure may not be major in the liquid crystal phase near c_A.

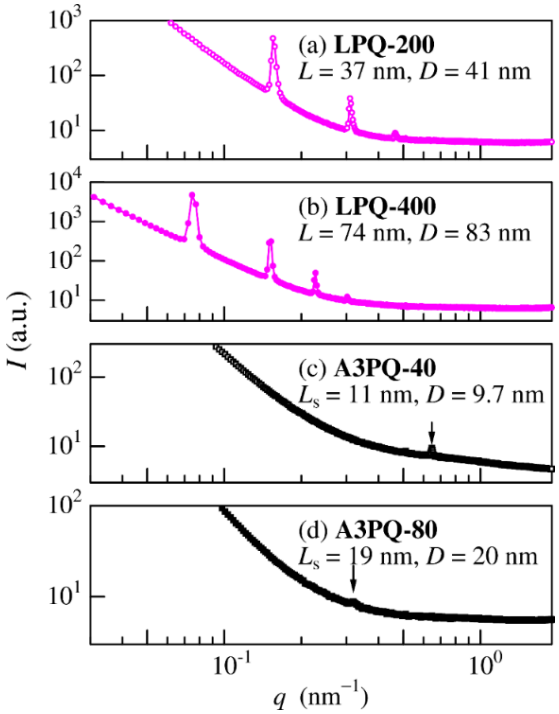

Figure 6. Angular dependence of scattering intensity I for (a) **LPQ-200** ($c = 0.40_2$ g cm^{-3}), **LPQ-400** ($c = 0.37_4$ g cm^{-3}), **A3PQ-40** ($c = 0.58_0$ g cm^{-3}), and **A3PQ-80** ($c = 0.45_8$ g cm^{-3}) all in THF at 25 °C.

Scaled Particle Theory (SPT) for LPQ. It is known that the phase boundary concentrations c_I and c_A for linear semiflexible polymers in solution can be successfully explained by the SPT theory based on the hard wormlike spherocylinder model.[10-16] This theory may be suitable to analyze phase boundary concentrations of LPQ samples in THF if we assume that the smectic superstructure found in the SAXS profile is negligible nearby phase boundary concentrations as depicted in the previous section. Here, we explain theoretical details of the SPT to extend it for the star polymer as described below. According to Sato and Teramoto,[10] the mixing Helmholtz energy ΔA of the solution including n hard wormlike spherocylinders with the contour length L and the diameter d of the cylinder is given by

$$\frac{\Delta A}{nk_{\mathrm{B}}T}=\frac{\mu^{\circ}}{k_{\mathrm{B}}T}-1+\ln\left(\frac{c'}{1-\upsilon c'}\right)+\frac{B}{2}\left(\frac{c'}{1-\upsilon c'}\right)+\frac{C}{3}\left(\frac{c'}{1-\upsilon c'}\right)^{2}+\sigma \tag{3}$$

where, k_{B} is the Boltzmann constant, T the absolute temperature. μ°, c', and υ are the standard chemical potential, the number concentration, and the volume [$= (\pi/4)(L - d)d^2 + (\pi/6)d^3$] of the spherocylinder, respectively. The molecular parameters B and C are defined by

$$B\equiv\tfrac{\pi}{2}\left(L-d\right)^{2}d\rho+6\upsilon \tag{4}$$

$$C\equiv\left(\upsilon+\tfrac{\pi}{12}d^{3}\right)\left(B-2\upsilon-\tfrac{\pi}{6}d^{3}\right) \tag{5}$$

with the excluded-volume reduction parameter ρ of the spherocylinder by the wormlike chain orientation, and σ expresses the orientation and conformational entropy loss by the wormlike chain orientation in the nematic phase. The parameters ρ and σ depend on the orientational distribution function. If one uses the Onsager trial function for the orientational distribution function, ρ and σ are calculated as functions of the degree of orientation α in the trial function,[39] given by

$$\rho=\frac{4}{\sqrt{\pi\alpha}}\left[1-\frac{30}{32\alpha}+\frac{210}{\left(32\alpha\right)^{2}}+\frac{1260}{\left(32\alpha\right)^{3}}\right] \tag{6}$$

$$\sigma=\ln\alpha-1+\pi\,\mathrm{e}^{-\alpha}+\tfrac{1}{3}N_{\mathrm{K}}\left(\alpha-1\right)+\tfrac{5}{12}\ln\left\{\cosh\left[\tfrac{2}{5}N_{\mathrm{K}}\left(\alpha-1\right)\right]\right\} \tag{7}$$

where N_{K} is the number of the Kuhn statistical segments defined as

$$N_{\mathrm{K}}=\lambda L \tag{8}$$

with the Kuhn segment length λ^{-1} of the wormlike chain. In the isotropic phase, $\rho = 1$ and $\sigma = 0$.

The osmotic pressure Π of the solution and the chemical potential μ of the spherocylinder in the solution are calculated from ΔA by

$$\Pi=-\left(\frac{\partial\Delta A}{\partial V}\right)_{T,n}=\frac{k_{\mathrm{B}}Tc'}{1-\upsilon c'}\left[1+\frac{B}{2}\left(\frac{c'}{1-\upsilon c'}\right)+\frac{2C}{3}\left(\frac{c'}{1-\upsilon c'}\right)^{2}\right] \tag{9}$$

$$\mu=\left(\frac{\partial\Delta A}{\partial n}\right)_{T,V}=\mu^{\circ}+\ln\left(\frac{c'}{1-\upsilon c'}\right)+B\left(\frac{c'}{1-\upsilon c'}\right)+C\left(\frac{c'}{1-\upsilon c'}\right)^{2}+\frac{\upsilon\Pi}{k_{\mathrm{B}}T}+\sigma \tag{10}$$

where V is the volume of the solution. When the isotropic and nematic phases with the polymer mass concentrations c_{I} and c_{A}, respectively, coexist in the above spherocylinder solution, the following equilibrium conditions must be fulfilled:

$$\Pi_{\mathrm{iso}}(c_{\mathrm{I}})=\Pi_{\mathrm{nem}}(c_{\mathrm{A}}) \tag{11}$$

$$\mu_{\mathrm{iso}}(c_{\mathrm{I}})=\mu_{\mathrm{nem}}(c_{\mathrm{A}}) \tag{12}$$

where the subscripts iso and nem indicate the quantities of the isotropic and nematic phases, respectively, and c is calculated from the number concentration c' by $c = c'M/N_{\mathrm{A}}$ with the molar mass M of the spherocylinder. Furthermore, in the equilibrium nematic phase, ΔA must be a minimum with respect to α:

$$\partial\Delta A/\partial\alpha=0 \tag{13}$$

The equations from 11 to 13 form ternary simultaneous equations to determine c_{I}, c_{A}, and α.

Comparison with Experimental Data of LPQ. The theoretical phase boundary concentrations c_{I} and c_{A} can be calculated in terms of the above mentioned SPT if the parameters L, λ^{-1}, and d are given. The obtained c_{I} and c_{A} can be compared with the experimental data when

we assume the incompressibility of the polymer solution around the atmospheric pressure. The first parameter L for LPQ is calculated from the experimental M_w along with the helix pitch (or helix rise) per residue h by

$$L = \frac{M_w h}{M_0} \tag{14}$$

Here, h and λ^{-1} were determined from the dilute solution properties to be 0.19 nm and 43 nm, respectively.[21] Thus, the adjustable parameter at comparison between theory and experiment for the phase boundary concentrations for LPQ is only the parameter d.

Figure 7 compares theoretical and experimental c_I and c_A for LPQ in THF. When d = 1.9 nm is chosen, good agreements between theory and experimental data are obtained both for c_I and c_A. The experimental phase gap is slightly broader than the theoretical curves. It is most likely due to a certain molar mass distribution of our polymer samples.[30] We may also estimate the thermodynamic chain diameter d_v from the partial specific volume $\bar{v}$ by

$$d_v = \sqrt{\frac{4M_0\bar{v}}{\pi N_A h}} \tag{15}$$

when the chain end effect is negligible. The calculated d_v value for LPQ is 1.73 nm which is substantially close to that of d = 1.9 nm. We consequently conclude that the isotropic-liquid crystal phase behavior of the LPQ-THF system is successfully explained by the current SPT theory for the wormlike spherocylinder with the parameters determined in dilute solution. In other words, the liquid crystallinity of the THF solution of LPQ arises from the reduction of the intermolecular excluded volume by the chain orientation, just like the other stiff polymer solutions.[10]

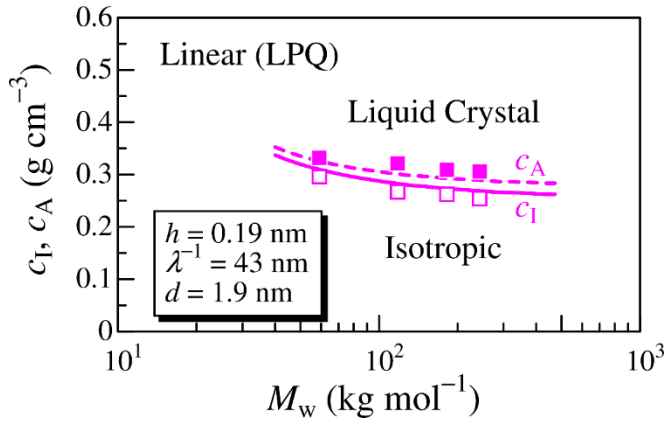

Figure 7. Comparison between experimental c_I (unfilled squares) and c_A (filled squares) for LPQ in THF at 25 °C and the theoretical values for c_I (solid curve) and c_A (dashed curve) with λ^{-1} = 43 nm, h = 0.19 nm, and d = 1.9 nm.

Modified SPT theory for Star Polymers. Under the single contact approximation,[40] ΔA of the isotropic solution including uniform 3-arm-star polymers of the total contour length L (= $3L_s$) and the diameter d is identified with that for the linear polymer given by eq 3. Although the three-arm star has three chain ends, the end effect on ΔA can be neglected if the arm chains are long enough. On the other hand, ΔA of the nematic solution of the 3-arm-star polymer cannot be approximated by that of the corresponding linear polymer, because the excluded volume for the 3-arm-star polymer taking the conformation in Figure 5(b) or (c) is definitely different from that for the linear polymer.

We assume here the two orientations of the star polymer as illustrated in Figure 8 as suggested in the above mentioned SAXS results with Figure 5; this is consistent with the dilute solution properties, that is, each arm connected with a rather flexible joint.[30] Case 1: Two arm chains align parallel and the star chain behaves as a cylindrical particle with the length of $2L_s$ (panel a). Case 2: All three arms align parallel with the length of L_s (panel b). Then, ΔA of the nematic solution may be approximated by that given by eq 3 where L and d are replaced by $L_{eff} = (2/3)L = (2/3)M_w h/M_0$ (Case 1) or $L_{eff} = (1/3)L = (1/3)M_w h/M_0$ (Case 2) and an effective diameter d_{eff} (*cf.* the dotted cylinders in Figure 8); the orientation-dependent parameter ρ is approximated by the same equation as eq 6. Furthermore, the chain orientation near the branch point may cost an excess Helmholtz energy, which must be included in the parameter σ. We here simply assume that σ has an extra constant term $\Delta\sigma$, replacing σ in eq 7 by

$$\sigma = \ln\alpha - 1 + \pi e^{-\alpha} + \frac{1}{3}N(\alpha - 1) + \frac{5}{12}\ln\left\{\cosh\left[\frac{2}{5}N(\alpha - 1)\right]\right\} + \Delta\sigma \qquad (16)$$

The phase boundary concentrations c_I and c_A as well as α were determined from the simultaneous eqs 11 – 13, where Π_{nem} and μ_{nem} are calculated from the above mentioned modified ΔA.

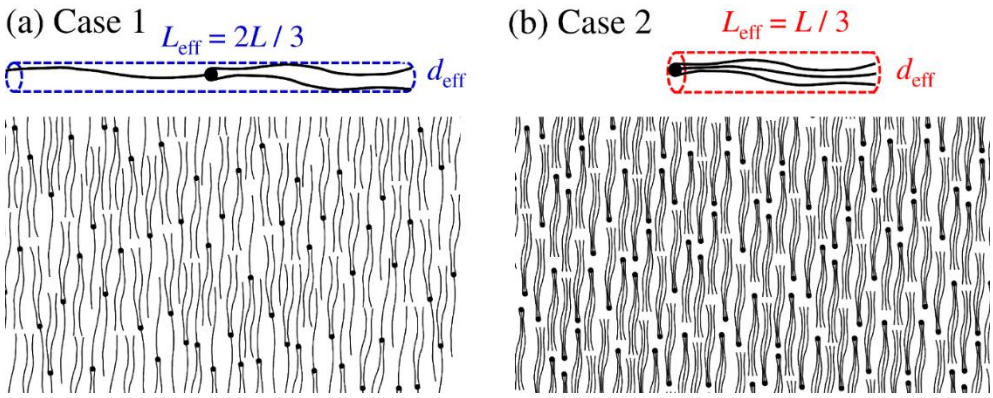

Figure 8. Schematic representation of the chain conformation of A3PQ chains in the nematic phase.

Let us compare theoretical values for the modified SPT with the experimental data. Here, we assumed the local conformation of each arm chain is the same as those for the linear analogue, that is, λ^{-1} = 43 nm, h = 0.19 nm, and d = 1.9 nm (in the isotropic phase), as well as M_0 = 0.300 kg mol^{-1}. The remaining adjustable parameters are thus d_{eff} and $\Delta\sigma$. When we chose d_{eff} = 2.4 nm and $\Delta\sigma$ = 20 for Case 1 or d_{eff} = 3.7 nm and $\Delta\sigma$ = 32 for Case 2, the theoretical values fit the experimental data almost quantitatively, as shown in Figure 9. It is however noticed that no numerical solution of the simultaneous equations were found for M_w larger than the right end of the theoretical curve at which the resultant theoretical phase boundary concentrations of the star polymers are close to those for the corresponding linear chain. This theoretically ill behavior may be due to the cylindrical model for the star polymer in the nematic phase (the dotted cylinder in Figure 8), although these mathematical difficulties can be escaped when d_{eff} is assumed to increase weakly with M_w. In any event, the agreement between theory and experiment in Figure 9 is satisfactorily good and the model used is suitable in the limited M_w region. The obtained d_{eff} values are reasonable since they should be larger than d (= 1.9 nm) of the LPQ single chain. Furthermore, the ratio $\Delta\sigma/\sigma$ is ca. 0.7 (Case 1) or ca. 0.9 (Case 2) in the equilibrium nematic phase, indicating that the contribution of $\Delta\sigma$ is considerably large, that is, the conformation of the star polymer in

the nematic phase illustrated in Figure 8 (the chain in the dotted cylinder), particularly for the Case 2, is entropically unfavorable. A further important point is that both Case 1 and Case 2 may explain the phase behavior. Taking the conformational entropy into consideration, both the two conformations can exist in the same nematic phase as illustrated in the TOC figure even though the Case 1 conformation may be major in the nematic phase because $\Delta\sigma$ is smaller than that for Case 2 while actual population cannot be determined from the current analysis.

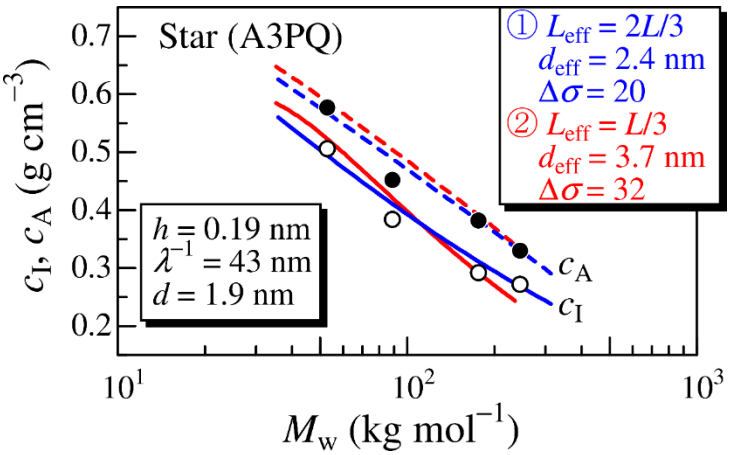

Figure 9. Comparison of the experimental c_I (solid curves) and c_A (dashed curves) for A3PQ in THF at 25 °C with the scaled particle theoretical values with the parameters listed in the Figure (curves).

Conclusions

THF solutions of both linear (LPQ) and 3-arm star (A3PQ) poly[5,8-dimethyl-6,7-bis(propoxymethyl)quinoxaline-2,3-diyl]s have lyotropic liquid crystallinity at high concentrations in the range of M_w from 50 to 250 kg mol^{-1}. Both phase boundary concentrations c_I and c_A for A3PQ exhibit much stronger M_w dependence, and are remarkably higher in the low M_w region than those for LPQ, clearly indicating that the chain architecture is definitely important for the isotropic-liquid crystal phase behavior at least for the low molar mass range. Smectic superstructure was also found for some low M_w samples at higher concentration than the biphasic region.

The obtained phase boundary concentrations for LPQ were successfully explained by the scaled particle theory (SPT) with the molecular parameters determined from the scattering methods in dilute THF solution as in the case of other stiff chains. The isotropic-liquid crystal phase diagram for A3PQ was also successfully explained by a modified SPT when we use the cylinder model illustrated in Figure 8 (the dotted cylinders) in the nematic phase. We conclude that the higher phase boundary concentrations for A3PQ than those for LPQ in the low M_w region arises from (1) the shorter contour length of the dotted cylinder for A3PQ than the LPQ chain in the nematic phase as well as (2) the higher entropic penalty of A3PQ at the nematic phase formation. At this moment, the actual chain conformation of A3PQ in the nematic phase has not been confirmed yet other than the weak but sharp diffraction at low q region. In order to explore further functionality of the liquid crystal phase of rigid star polymers, investigation of the conformational properties in the nematic (and/or the smectic phase) is an important research topic.

Acknowledgments

We are grateful to Dr. Noboru Ohta (SPring-8), Dr. Noriyuki Igarashi (KEK), and Dr. Nobutaka Shimizu (KEK) for SAXS measurements. This work was partially supported by JSPS KAKENHI Grant Nos. JP17K05884 and JP18H02020. The SAXS data were acquired at the BL40B2 beamline in SPring-8 with the approval of the Japan Synchrotron Radiation Research Institute (JASRI) (Proposal Nos. 2017A1082 and 2017B1062) and at the BL-6A beamline in KEK-PF under the approval of the Photon Factory Program Advisory Committee (Proposal No. 2017G023).

References

1. Shibaev, V. 1.10 - Liquid Crystalline Polymers. In *Polymer Science: A Comprehensive Reference*, Matyjaszewski, K.; Möller, M., Eds. Elsevier: Amsterdam, 2012; pp 259-285.
2. Kwolek, S. L.; Morgan, P. W.; Schaefgen, J. R.; Gulrich, L. W. Synthesis, Anisotropic Solutions, and Fibers of Poly(1,4-Benzamide). *Macromolecules* **1977**, *10*, 1390-1396.
3. Aharoni, S. M. Rigid Backbone Polymers .2. Polyisocyanates and Their Liquid-Crystal Behavior. *Macromolecules* **1979**, *12*, 94-103.
4. Itou, T.; Teramoto, A. Isotropic Liquid-Crystal Phase-Equilibrium in Solutions of Semiflexible Polymers - Poly(Hexyl Isocyanate). *Macromolecules* **1988**, *21*, 2225-2230.
5. Sato, T.; Sato, Y.; Umemura, Y.; Teramoto, A.; Nagamura, Y.; Wagner, J.; Weng, D. X.; Okamoto, Y.; Hatada, K.; Green, M. M. Polyisocyanates and the Interplay of Experiment and Theory in the Formation of Lyotropic Cholesteric States. *Macromolecules* **1993**, *26*, 4551-4559.
6. Green, M. M.; Zanella, S.; Gu, H.; Sato, T.; Gottarelli, G.; Jha, S. K.; Spada, G. P.; Schoevaars, A. M.; Feringa, B.; Teramoto, A. Mechanism of the transformation of a stiff polymer lyotropic nematic liquid crystal to the cholesteric state by dopant-mediated chiral information transfer. *J. Am. Chem. Soc.* **1998**, *120*, 9810-9817.
7. Kim, J.; Novak, B. M.; Waddon, A. J. Lyotropic Liquid Crystalline Properties of Poly(N,N‘-di-n-hexylguanidine). *Macromolecules* **2004**, *37*, 1660-1662.
8. Kim, J.; Novak, B. M.; Waddon, A. J. Liquid crystalline properties of polyguanidines. *Macromolecules* **2004**, *37*, 8286-8292.
9. Ciferri, A. *Liquid crystallinity in polymers : principles and fundamental properties*. VCH Publishers: 1991; p x, 438 p.
10. Sato, T.; Teramoto, A. Concentrated solutions of liquid-crystalline polymers. *Adv. Polym. Sci.* **1996**, *126*, 85-161.
11. Maeno, K.; Nakamura, Y.; Terao, K.; Sato, T.; Norisuye, T. Liquid crystallinity of concentrated solutions of polymacromonomers consisting of polystyrene. *Kobunshi Ronbunshu* **1999**, *56*, 254-259.
12. Nakamura, Y.; Koori, M.; Li, Y.; Norisuye, T. Lyotropic liquid crystal formation of polystyrene polymacromonomers in dichloromethane. *Polymer* **2008**, *49*, 4877-4881.
13. Natsume, T.; Wu, L. B.; Sato, T.; Terao, K.; Teramoto, A.; Fujiki, M. Chain-stiffness and lyotropic liquid crystallinity of polysilylene bearing (S)-2-methylbutyl and n-decyl substituents. *Macromolecules* **2001**, *34*, 7899-7904.
14. Sato, T.; Shimizu, T.; Kasabo, F.; Teramoto, A. Isotropic−Cholesteric Phase Equilibrium in Solutions of Cellulose Tris(phenyl carbamate). *Macromolecules* **2003**, *36*, 2939-2943.
15. Kuse, Y.; Asahina, D.; Nishio, Y. Molecular Structure and Liquid-Crystalline Characteristics of Chitosan Phenylcarbamate. *Biomacromolecules* **2009**, *10*, 166-173.

16. Oyamada, K.; Terao, K.; Suwa, M.; Kitamura, S.; Sato, T. Lyotropic Liquid Crystallinity of Armylose Tris(alkylcarbamates): Cholesteric and Smectic Phase Formation in Different Solvents. *Macromolecules* **2013**, *46*, 4589-4595.
17. Ito, Y.; Ihara, E.; Murakami, M.; Sisido, M. Studies on the conformation of helical poly(2,3-quinoxalines). Empirical energy calculation and theoretical circular dichroism. *Macromolecules* **1992**, *25*, 6810-6813.
18. Yamamoto, T.; Yamada, T.; Nagata, Y.; Suginome, M. High-molecular-weight polyquinoxaline-based helically chiral phosphine (PQXphos) as chirality-switchable, reusable, and highly enantioselective monodentate ligand in catalytic asymmetric hydrosilylation of styrenes. *J. Am. Chem. Soc.* **2010**, *132*, 7899-901.
19. Yamamoto, T.; Akai, Y.; Nagata, Y.; Suginome, M. Highly enantioselective synthesis of axially chiral biarylphosphonates: asymmetric Suzuki-Miyaura coupling using high-molecular-weight, helically chiral polyquinoxaline-based phosphines. *Angew. Chem. Int. Ed.* **2011**, *50*, 8844-7.
20. Akai, Y.; Yamamoto, T.; Nagata, Y.; Ohmura, T.; Suginome, M. Enhanced catalyst activity and enantioselectivity with chirality-switchable polymer ligand PQXphos in Pd-catalyzed asymmetric silaborative cleavage of meso-methylenecyclopropanes. *J. Am. Chem. Soc.* **2012**, *134*, 11092-5.
21. Nagata, Y.; Hasegawa, H.; Terao, K.; Suginome, M. Main-Chain Stiffness and Helical Conformation of a Poly(quinoxaline-2,3-diyl) in Solution. *Macromolecules* **2015**, *48*, 7983-7989.
22. Murakami, H.; Norisuye, T.; Fujita, H. Dimensional and Hydrodynamic Properties of Poly(Hexyl Isocyanate) in Hexane. *Macromolecules* **1980**, *13*, 345-352.
23. Kuwata, M.; Murakami, H.; Norisuye, T.; Fujita, H. Intrinsic-Viscosity of Poly(Hexyl Isocyanate) in Butyl Chloride. *Macromolecules* **1984**, *17*, 2731-2734.
24. Itou, T.; Chikiri, H.; Teramoto, A.; Aharoni, S. M. Wormlike Chain Parameters of Poly(Hexyl Isocyanate) in Dilute-Solution. *Polym. J.* **1988**, *20*, 143-151.
25. Nagata, Y.; Takagi, K.; Suginome, M. Solid polymer films exhibiting handedness-switchable, full-color-tunable selective reflection of circularly polarized light. *J. Am. Chem. Soc.* **2014**, *136*, 9858-61.
26. Ito, Y.; Ihara, E.; Uesaka, T.; Murakami, M. Synthesis of Novel Thermotropic Liquid Crystalline Poly(2,3-quinoxalines). *Macromolecules* **1992**, *25*, 6711-6713.
27. Zakharova, S. S.; Jesse, W.; Backendorf, C.; van der Maarel, J. R. Liquid crystal formation in supercoiled DNA solutions. *Biophys. J.* **2002**, *83*, 1119-29.
28. Terao, K.; Shigeuchi, K.; Oyamada, K.; Kitamura, S.; Sato, T. Solution Properties of a Cyclic Chain Having Tunable Chain Stiffness: Cyclic Amylose Tris(*n*-butylcarbamate) in Θ and Good Solvents. *Macromolecules* **2013**, *46*, 5355-5362.
29. Goodson, S. H.; Novak, B. M. Synthesis and Characterization of Wormlike Three-arm Poly(*n*-hexyl isocyanate) Star Polymers. *Macromolecules* **2001**, *34*, 3849-3855.
30. Hasegawa, H.; Nagata, Y.; Terao, K.; Suginome, M. Synthesis and Solution Properties of a Rigid Helical Star Polymer: Three-Arm Star Poly(quinoxaline-2,3-diyl). *Macromolecules* **2017**, *50*, 7491-7497.
31. Pasch, H. 2.03 - Chromatography A2 - Matyjaszewski, Krzysztof. In *Polymer Science: A Comprehensive Reference*, Möller, M., Ed. Elsevier: Amsterdam, 2012; pp 33-64.
32. Gu, H.; Nakamura, Y.; Sato, T.; Teramoto, A.; Green, M. M.; Andreola, C. Global conformations of chiral polyisocyanates in dilute solution. *Polymer* **1999**, *40*, 849-856.

33. Farmer, B. S.; Terao, K.; Mays, J. W. Characterization of model branched polymers by multi-detector SEC in good and theta solvents. *Int. J. Polym. Anal. Charact.* **2006**, *11*, 3-19.
34. Shimizu, N.; Yatabe, K.; Nagatani, Y.; Saijyo, S.; Kosuge, T.; Igarashi, N. Software Development for Analysis of Small-angle X-ray Scattering Data. *AIP Conf. Proc.* **2016**, *1741*, 050017.
35. Terao, K.; Okumoto, M.; Nakamura, Y.; Norisuye, T.; Teramoto, A. Light-scattering and phase-separation studies on cyclohexane solutions of four-arm star polystyrene. *Macromolecules* **1998**, *31*, 6885-6890.
36. Tasaka, Y.; Okumoto, M.; Nakamura, Y.; Norisuye, T. Light Scattering and Phase Separation Studies on Cyclohexane Solutions of Six-Arm Star Polystyrene. *Polym. J.* **2008**, *40*, 634-639.
37. Yu, S. M.; Conticello, V. P.; Zhang, G.; Kayser, C.; Fournier, M. J.; Mason, T. L.; Tirrell, D. A. Smectic ordering in solutions and films of a rod-like polymer owing to monodispersity of chain length. *Nature* **1997**, *389*, 167-170.
38. Okoshi, K.; Kamee, H.; Suzaki, G.; Tokita, M.; Fujiki, M.; Watanabe, J. Well-Defined Phase Sequence Including Cholesteric, Smectic A, and Columnar Phases Observed in a Thermotropic LC System of Simple Rigid-Rod Helical Polysilane. *Macromolecules* **2002**, *35*, 4556-4559.
39. Onsager, L. The Effects of Shape on the Interaction of Colloidal Particles. *Ann. N.Y. Acad. Sci.* **1949**, *51*, 627-659.
40. Sato, T.; Jinbo, Y.; Teramoto, A. Intermolecular interaction of stiff-chain polymers in solution. *Macromolecules* **1997**, *30*, 590-596.

For Table of Contents Use Only

Lyotropic Liquid Crystallinity of Linear and Star Poly(quinoxaline-2,3-diyl)s: Isotropic–Liquid Crystal Phase Equilibria in Tetrahydrofuran

Hirokazu Hasegawa, Ken Terao, Takahiro Sato, Yuuya Nagata, and Michinori Suginome